Multispectral Management of the Photon Orbital Angular Momentum

Mikaël Ghadimi Nassiri and Etienne Brasselet*
Université de Bordeaux, CNRS, LOMA, UMR 5798, F-33400 Talence, France

(Received 21 August 2018; published 20 November 2018)

We report on a programmable liquid crystal spatial light modulator enabling independent orbital angular momentum state control on multiple spectral channels. This is done by using electrically controllable "topological pixels" that independently behave as geometric phase micro-optical elements relying on self-engineered liquid crystal defects. These results open interesting opportunities in optical manipulation, sensing, imaging, and communications, as well as information processing. In particular, spectral vortex modulation allows considering singular spatiotemporal shaping of ultrashort pulses which may find applications in many areas such as material processing, spectroscopy, or elementary particles acceleration.

DOI: 10.1103/PhysRevLett.121.213901

Photonics technologies provide our societies with tools to better see and understand our world and explore others, but also to improve health care, manufacturing, and ways to inform and communicate. For more than two decades, the sought-after management of the photon orbital angular momentum has continued to foster many opportunities [1,2]. Spatial light modulators (SLMs) refer to optical devices enabling spatiotemporal modulation of the phase, polarization, or amplitude of light fields. Many technologies have been developed since the 1980s, liquid crystals (LCs) are prime choice materials owing to their great sensitivity to external fields and their high birefringence. Electrically controlled liquid crystal spatial light modulators (LC-SLMs) imposed themselves in many areas whenever structured light is needed, see, for instance, [3,4], which nowadays covers a broad range of topics [2]. A conventional LC-SLM typically consists of a two-dimensional matrix made of up to several megapixels, each of them behaving as an electrically controlled optical retarder characterized by a uniform optical axis orientation angle ψ_0, see Fig. 1(a). Depending on the incident polarization state and postpolarization filtering, versatile modulation of light is, thus, obtained.

Another option towards structuring light fields consists of exploiting the geometric phase spatial modulations associated with inhomogeneous anisotropic optical elements [5]. Noting that LC-based materials are widely used to fabricate geometric phase optical elements [6,7], what if the independent assets of SLMs and geometric phase are combined? This would give access to spatial light modulation at the level of a pixel, hence, opening novel beam shaping possibilities, since geometric phase is basically wavelength independent. To do so, one would need pixels enabling controllable phase modulation. Such a device does not yet exist, and here, we propose a step forward to this aim, by using a LC-SLM whose pixel action on light is of a geometric nature. Here, we choose a specific pixel design that consists of in-plane optical axis orientation given by $\psi = q\phi$ with $q \in \mathbb{Z}/2$, see Fig. 1(b), which is the microscopic counterpart of macroscopic so-called q plates [8]. The key feature of such elements is to enable isomorphic mapping from the two-dimensional polarization space to the two-dimensional subspace defined by a pair of opposite orbital angular momentum eigenvalues $\ell = \pm 2q$, which proved to be a powerful tool both in classical and quantum optics [9]. Of course, it could be argued that choosing a hard-coded design for individual pixels has an inherent limitation. However, as shown here, such a step already provides for spectrally agile beam shaping capabilities that cannot be achieved with existing optical systems. By doing so, this work not only brings a technical advance in the field of optics and photonics, but also offers a novel generic approach for manipulating the spatial degrees of freedom of waves.

Considering an array of electrically controlled q plates, the multispectral management of the photon orbital angular momentum is possible, as depicted in Fig. 2(a). The working

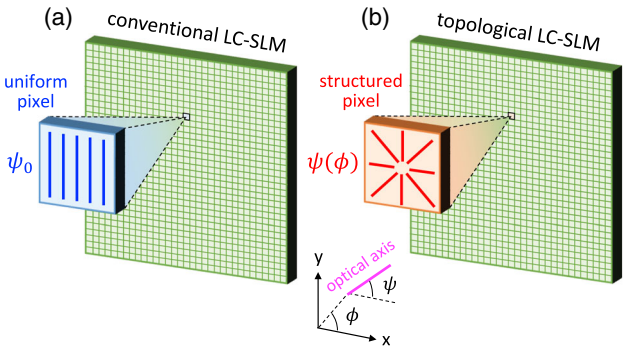

FIG. 1. (a) Illustration of a usual optical device made of a two-dimensional matrix of electrically controlled liquid crystal pixels having a uniform molecular orientation, $\psi = \psi_0$. (b) Topological counterpart where every pixel acts as an electrically controlled microscopic q plate ($q = +1$ for the enlarged pixel).

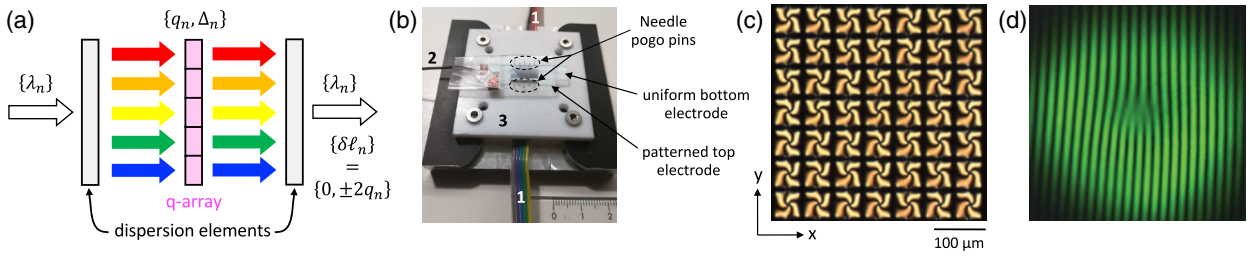

FIG. 2. (a) Multispectral modulation of the orbital angular momentum content of a discrete spectral channel λ_n by an array of q plates of order q_n. (b) Fabricated LC-SLM based on self-engineered electrically controlled LC topological defects with $q = +1$. The ruler is in centimeter units. (1) 2×5 electrical cables supplying applied voltage; (2) ground; (3) Teflon holder. Top Teflon holder not shown here. (c) Typical observation of a matrix of 49 q plates observed between crossed linear polarizers and white light incoherent illumination. (d) Interferometric demonstration of the orbital angular momentum state change by an increment of two units performed by an individual structured pixel, here, at 550 nm wavelength. The forked pattern results from the far-field superposition of a processed circularly polarized Gaussian beam with a reference Gaussian beam.

principle of the device is obtained by generalizing the monochromatic behavior of a q plate [8] to a polychromatic field that consists of discrete wavelengths λ_n. For this, we introduce the circular polarization basis $(\mathbf{c}_+, \mathbf{c}_-)$ where $\mathbf{c}_\sigma = (\mathbf{x} + i\sigma\mathbf{y})/\sqrt{2}$ with $\sigma = \pm 1$ the photon helicity. Neglecting the propagation factor, we express the input light field as $\mathbf{E}_{\text{in}} = \sum_{\lambda_n} E_n(a_n\mathbf{c}_+ + b_n\mathbf{c}_-)$ and, discarding the diffraction inside each element, the output field is expressed as

$$\mathbf{E}_{\text{out}} = \sum_{\lambda_n} E_n e^{i\Phi_n} \begin{pmatrix} \cos\frac{\Delta_n}{2} & i\sin\frac{\Delta_n}{2} e^{-i\ell_n\phi} \\ i\sin\frac{\Delta_n}{2} e^{+i\ell_n\phi} & \cos\frac{\Delta_n}{2} \end{pmatrix} \begin{pmatrix} a_n \\ b_n \end{pmatrix}, \tag{1}$$

where $\Phi_n = \pi(L/\lambda_n)(n_\parallel + n_\perp)$ is the dynamic phase and $\Delta_n = 2\pi(L/\lambda_n)(n_\parallel - n_\perp)$ is the birefringence phase retardation, with $n_\parallel$ and $n_\perp$ being the refractive indices along and perpendicular to the optical axis, and $\ell_n = 2q_n$. Note that Eq. (1) is only slightly perturbed by the finite practical width $\delta\lambda_n$ of the channels provided that $\delta\lambda_n/\lambda_n \ll 1$. The orbital angular state of the σ-polarized channel n is, therefore, modified by an increment of $2\sigma q_n$ when $\Delta_n = (2m+1)\pi$, $m \in \mathbb{N}$, while it remains unaffected when $\Delta_n = 2m\pi$.

The realization of a topological LC-SLM raises serious manufacturing challenges although LC structuring technologies are mature at the macroscopic scale for the production of electrically tunable single [10] or arrays [11] of electrically controlled q plates. Indeed, the extension of existing machining techniques to the creation of structured pixels with lateral size of the order of ~ 10 μm, which, nowadays, is the typical pixel size of LC-SLM, is yet to be validated. We address this issue by implementing a nature-assisted approach originally developed using LC droplets [12] and further extended to LC films [13]. Following a preliminary demonstration of a linear array of self-engineered microscopic $+1$ plates without individual control [14], here, we fabricate a device that consists of a 10×127 matrix of 50×50 μm square-shaped q pixels, where the 10 lines can be electrically controlled independently. The device is prepared by sandwiching a thin film (typical thickness of the order of 10 μm) of nematic LC with negative dielectric anisotropy between two transparent and conductive indium-tin-oxide coated glass slabs treated to ensure perpendicular anchoring of the LC molecules using cetyl-trimethyl-ammonium bromide surfactant. Electrode patterning is achieved by direct laser ablation [15] performed before assembling the LC cell. Without applied voltage, the LC molecules remain aligned perpendicularly to the plane of the sample ($\Delta = 0$ for all pixels). The sample used in Fig. 3 has a thickness of $\simeq 13$ μm and is made of the nematic liquid crystal mixture MLC-6608 (Merck) and the sample used in Fig. 4 has a thickness of $\simeq 7$ μm and is made of the nematic liquid crystal mixture DFLNC (Beam Co).

Above a threshold voltage of the order of a few Volts, the LC spontaneously forms one umbilical defect per pixel which can be assessed by observation between crossed linear polarizers, as shown in Fig. 2(c). There, the twisted extinction crosses, whose right or left handedness is randomly selected as the defect is spontaneously generated from the unperturbed initial LC state, are a generic manifestation of localized umbilical nematic LC defects with $q = +1$ resulting from the elastic anisotropy of the LC [16,17]. This modifies the wavefront curvature without altering the orbital angular momentum control operated by every topological pixel. This is ascertained by interferometric analysis of the output light field that reveals a structured phase factor $\exp(2i\sigma\phi)$, see Fig. 2(d), as expected from Eq. (1).

As a first demonstration, we report on ultrabroadband scalar and vectorial vortex beam shaping. This is done by choosing $\Delta_n = \pi$ for all n, hence, obtaining pure vortex generation independently of the incident polarization state according to Eq. (1). The experimental implementation is depicted in Fig. 3(a). In practice, we use a supercontinuum laser source dispersed by a blazed grating and recollimated onto an array of optical fibers that define the spectral

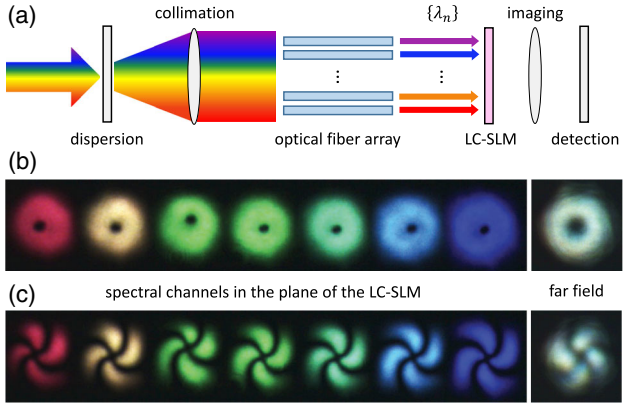

FIG. 3. (a) Sketch of the experimental setup for ultrabroadband scalar and vectorial vortex beam shaping. The optical fiber array consists of 12 multimode step-index fibers with numerical aperture 0.2 and core radius 50 μm. The detection system is either a camera or a fiber spectrometer. Scalar vortex (b) and vectorial (c) beam shaping when incident light is, respectively, circularly and linearly polarized. In both cases, the observation is made by placing an output polarizer that selects the polarization state orthogonal to the incident one. The image on the left corresponds to the seven spectral channels $\lambda_n = 485$, 511, 533, 555, 575, 595, and 617 nm with ~10 nm full width at half maximum in the plane of the LC-SLM and the image on the right refers to the far field of the polychromatic structured light field.

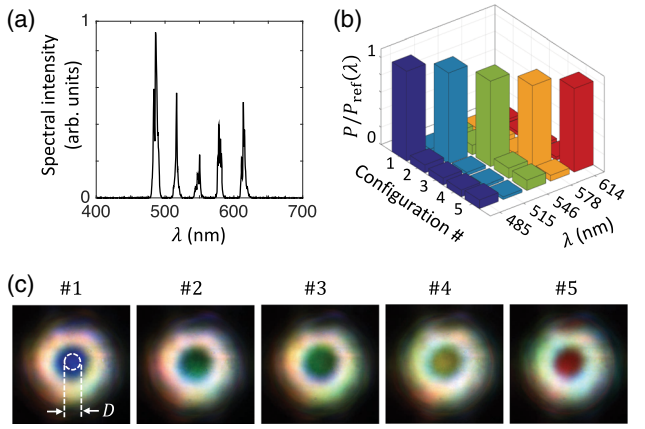

FIG. 4. Demonstration of on-demand polychromatic superposition of orbital angular momentum states. (a) Spectrum of the incident light that consists of five spectral channels at $\lambda_n = 485$, 515, 546, 578, and 614 nm. (b) Chart of the on-axis power P collected with a fiber spectrometer having a clear aperture of diameter $D = 200$ μm, see leftmost panel (c) for the five chosen configurations labeled #m, with $m = (1, 2, 3, 4, 5)$. The vortex states of every channel is optimized for $\Delta_n^{\mathrm{vortex}} = 7\pi$, 7π, 5π, 5π, and 5π, respectively. The nonvortex states correspond to $\Delta_n^{\mathrm{nonvortex}} = \Delta_n^{\mathrm{vortex}} - \pi$. The collected power values are normalized to the reference power $P_{\mathrm{ref}}(\lambda)$ associated to the nonvortex state. (c) Total far-field intensity profiles for the five configurations.

channels. Multispectral scalar vortex shaping is achieved by using an incident circular polarization state, namely, $(a_n = 1, b_n = 0)$ or $(a_n = 0, b_n = 1)$ for all n, which, respectively, gives $\mathbf{E}_{\mathrm{out}} \propto e^{2i\sigma\phi}\mathbf{c}_{-\sigma}$. The results are shown in Fig. 3(b). On the other hand, vectorial beam shaping is achieved by using an incident linear polarization state, namely, $|a_n| = |b_n|$ for all n, which gives a polychromatic nonseparable spin-orbit state $\mathbf{E}_{\mathrm{out}} \propto e^{-2i\phi}\mathbf{c}_+ + e^{+2i\phi}\mathbf{c}_-$. The results are shown in Fig. 3(c) where observations are made by placing a linear polarizer at the output of the device in order to reveal the vectorial nature of the proceed light beam. These experiments emphasize both the broadband and geometric phase features of our topological LC-SLM. Importantly, the present approach allows one-to-one mapping between the Poincaré sphere of polarization and the high-order Poincaré sphere of order ℓ [18] for all wavelengths. This solves previous optical state dispersion drawbacks associated with the global processing of the whole spectrum using "Bragg-Berry" optical elements [19].

Note that broadband optical vortex generation based on geometric phase has been reported using various approaches [20–28]; however, none of them enables spectral agility of the associated photon orbital angular momentum. Here, wavelength-dependent orbital angular momentum control is also achieved, as illustrated in Fig. 4, where on-demand activation or deactivation of on-axis intensity of any spectral component of a polychromatic field is demonstrated. In the context of optical nanoscopy [29], this allows us to consider spectrally agile stimulation-emission-depletion (STED) super-resolved imaging. Indeed, the wavelength(s) of the on-axis reading light can be adapted to the fluorescence characteristics of the scrutinized sample. Straightforwardly, this can also be deployed in STED-inspired optical techniques, for instance, in the field of optical nanolithography where the spatial resolution of three-dimensional direct laser writing techniques can be improved [30]. We also propose another important application, that is, the four-dimensional shaping of ultrafast optical pulses. Optical pulse shaping is a mature technology having a huge range of applications, for instance, in spectroscopy and light wave communications [31] that still continue to be developed, as illustrated, for instance, by recent works on spatiotemporal focusing [32–34]. Situations involving the optical orbital angular momentum are also attractive in high-energy optics where techniques are developed towards space-time manipulation of optical pulses [35–37]. Hereafter, we discuss a case study illustrating how spectral vortex modulation is likely to impact this field.

The basic scheme relies on Fourier-transform pulse shaping. It consists in decomposing an incident pulse into its constituent spectral components that are individually modulated. Once recombined, the spectral components reconstruct an output waveform given by the Fourier transform of the reshaped spectrum. For the purpose of demonstration, we consider an incident chirped Gaussian pulse described by the temporal waveform amplitude

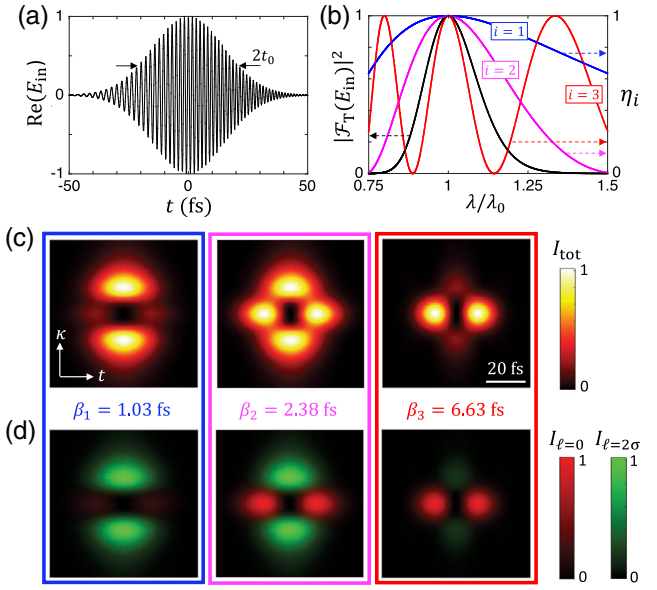

FIG. 5. Four-dimensional optical pulse shaping by spectral vortex modulation. (a) Electric field temporal waveform of a chirped ultrashort optical Gaussian pulse characterized by central wavelength $\lambda_0 = 500$ nm, spatial waist $r_0 = 500$ μm, temporal waist $t_0 = 21$ fs, and chirp parameter $\delta\omega = 0.60$ rad/fs, whose intensity spectrum is shown in panel (b) (black curve). The spectral dependence of the optical vortex purity for three cases, η_i with $i = (1, 2, 3)$, is shown in panel (b) (colored curves). (c) Total far field intensity profile of the spatiotemporally shaped pulse for the three cases, which are associated with parameters β_i, in the case $q = +1$. An optical bottle pulse is obtained for $i = 2$ while only transverse and longitudinal spatial modulation is obtained for $i = 1$ and $i = 3$, respectively. κ refers to the spatial frequencies in the transverse plane (arbitrary units). (d) Intensity profiles of the field component carrying distinct orbital angular momentum per photon, here $0\hbar$ (red color) and $2\sigma\hbar$ (green color) per photon.

$E_{\mathrm{in}}(r,t) = E_0 e^{-r^2/r_0^2 + i\omega_0 t - \alpha t^2}$ with $\alpha = 1/t_0^2 - i\delta\omega/(2t_0)$, where ω_0 is the central angular frequency, and r_0 and t_0 are, respectively, the spatial and temporal characteristic pulse widths, see Fig. 5(a). In addition, $\delta\omega$ characterizes the instantaneous angular frequency shift at t_0, noting that $\omega(t) = \omega_0 + (t/t_0)\delta\omega$. The corresponding intensity spectrum $|\mathcal{F}_T[E_{\mathrm{in}}]|^2$ is shown as the black curve in Fig. 5(b), where $\mathcal{F}_T$ refers to the temporal Fourier transform. Then, we consider the ideal hyperspectral (i.e., spectrally continuous) situation in the simple case of a retardance having a linear spectral dependence of the form $\Delta(\omega) = \pi + \beta(\omega - \omega_0)$. This implies that the central frequency ω_0 is fully converted into a vortex state while others experience partial vortex transformation according to the frequency-dependent purity parameter $\eta(\omega) = \sin^2[\Delta(\omega)/2]$. The latter characterizes the fraction of the incident energy of a σ-circularly polarized incident pulse that is transformed into an orbital state $\ell = 2\sigma q$. By doing so, it is possible to create the pulsed analog of continuous-wave bottle beams [38]—an optical bottle pulse. The demonstration is shown in Fig. 5(c), where an optical pulse with a dark focus surrounded by regions of higher intensity can be created for an appropriate value of the parameter β, here, in the particular case $q = +1$. The calculations are made accounting for Eq. (1) taking a σ-polarized incident pulse. This gives rise to a superposition of a $\pm\sigma$-polarized field emerging from the topological pulse shaper. Namely, $\mathbf{E}_{\mathrm{out}}(r,t) = \mathcal{F}_T^{-1}[\mathcal{F}_T[E_{\mathrm{in}}]\cos(\Delta(\omega)/2)]\mathbf{c}_\sigma + i\mathcal{F}_T^{-1}[\mathcal{F}_T[E_{\mathrm{in}}]\sin(\Delta(\omega)/2)]e^{2i\sigma q\phi}\mathbf{c}_{-\sigma}$, where $\mathcal{F}^{-1}$ refers to the inverse Fourier transform. The far field then gives the optical bottle pulse described by $\mathcal{F}_S[\mathbf{E}_{\mathrm{out}}(r,t)]$, where $\mathcal{F}_S$ refers to the spatial Fourier transform. Note that the latter calculation implies that the dynamic phase factor in Eq. (1) does not play a role, which can be met in principle using compensation techniques before topological processing or by elaborating dynamic phase independent geometric phase elements following a recent approach [39]. Interestingly, the optical bottle pulse is associated with a nonstationary spin and orbital angular momentum, which can find uses in contactless optorheological studies based on light-matter angular momentum transfer. This is illustrated in Fig. 5(d) where the respective contributions of the field components carrying different orbital contents are depicted as distinct colors. This, obviously, opens further possibilities for four-dimensional pulse shaping once other configurations are considered.

Finally, we note that the quality of the geometric phase shaping provided by the topological liquid crystal pixels inherently benefits from the high-purity performances of umbilical defects, as demonstrated early in Ref. [13]. The limitation comes from the finite size of the pixel, and a key practical parameter is the ratio pixel size/defect core size. In the present case, the purity typically ranges from 0.8 up to more than 0.95 depending on the operating conditions. In addition, the efficiency of the process (i.e., the fraction of incident photons that can actually be processed) also depends on the unwanted Fresnel reflections of the substrates, which could be optimized by appropriate broadband coatings. On the other hand, the speed of the proposed liquid crystal device is basically that of a usual liquid crystal pixel in displays and may reach up to the kHz frequency for thin pixel thickness using conventional nematics.

The programmable manipulation of light, both in space and time, via the spectral management of the photon orbital angular momentum provides for a very large set of prospective applications, from continuous light waves to ultrashort optical pulses. Moreover, its general principle can be formally adapted to any wavelength range. Spectral vortex modulation is likely to impact many research areas such as optical imaging, quantum optical information, optical communications, optical spectroscopy, optical manipulation, or high-energy physics. Also, since optical phase singularities are a generic feature of wave physics, the proposed approach can be further extended to other

kinds of waves, such as sound, which might lead to the elaboration of novel noninvasive imaging tools for medical applications.

This study has been carried out with financial support from the French National Research Agency (Project No. ANR-15-CE30-0018), DGA, and Conseil Régional d'Aquitaine.

*etienne.brasselet@u-bordeaux.fr

[1] M. J. Padgett, Orbital angular momentum 25 years on, Opt. Express **25**, 11265 (2017).
[2] H. Rubinsztein-Dunlop, A. Forbes, M. V. Berry, M. R. Dennis, D. L. Andrews, M. Mansuripur, C. Denz, C. Alpmann, P. Banzer, T. Bauer *et al.*, Roadmap on structured light, J. Opt. **19**, 013001 (2017).
[3] C. Maurer, A. Jesacher, S. Bernet, and M. Ritsch-Marte, What spatial light modulators can do for optical microscopy, Laser Photonics Rev. **5**, 81 (2011).
[4] A. Forbes, A. Dudley, and M. McLaren, Creation and detection of optical modes with spatial light modulators, Adv. Opt. Photonics **8**, 200 (2016).
[5] R. Bhandari, Polarization of light and topological phases, Phys. Rep. **281**, 1 (1997).
[6] P. Chen, B.-Y. Wei, W. Ji, S.-J. Ge, W. Hu, F. Xu, V. Chigrinov, and Y.-Q. Lu, Arbitrary and reconfigurable optical vortex generation: A high-efficiency technique using director-varying liquid crystal fork gratings, Photon. Res. **3**, 133 (2015).
[7] J. Kim, Y. Li, M. N. Miskiewicz, C. Oh, M. W. Kudenov, and M. J. Escuti, Fabrication of ideal geometric-phase holograms with arbitrary wavefronts, Optica **2**, 958 (2015).
[8] L. Marrucci, C. Manzo, and D. Paparo, Optical Spin-to-Orbital Angular Momentum Conversion in Inhomogeneous Anisotropic Media, Phys. Rev. Lett. **96**, 163905 (2006).
[9] L. Marrucci, E. Karimi, S. Slussarenko, B. Piccirillo, E. Santamato, E. Nagali, and F. Sciarrino, Spin-to-orbital conversion of the angular momentum of light and its classical and quantum applications, J. Opt. **13**, 064001 (2011).
[10] S. Slussarenko, A. Murauski, T. Du, V. Chigrinov, L. Marrucci, and E. Santamato, Tunable liquid crystal q-plates with arbitrary topological charge, Opt. Express **19**, 4085 (2011).
[11] S. V. Serak, D. E. Roberts, J.-Y. Hwang, S. R. Nersisyan, N. V. Tabiryan, T. J. Bunning, D. M. Steeves, and B. R. Kimball, Diffractive waveplate arrays, J. Opt. Soc. Am. B **34**, B56 (2017).
[12] E. Brasselet, N. Murazawa, H. Misawa, and S. Juodkazis, Optical Vortices from Liquid Crystal Droplets, Phys. Rev. Lett. **103**, 103903 (2009).
[13] E. Brasselet and C. Loussert, Electrically controlled topological defects in liquid crystals as tunable spin-orbit encoders for photons, Opt. Lett. **36**, 719 (2011).
[14] C. Loussert, K. Kushnir, and E. Brasselet, Q-plates microarrays for parallel processing of the photon orbital angular momentum, Appl. Phys. Lett. **105**, 121108 (2014).
[15] A. Risch and R. Hellmann, Picosecond laser patterning of ITO thin films, Phys. Procedia **12**, 133 (2011).
[16] R. Barboza, U. Bortolozzo, M. G. Clerc, S. Residori, and E. Vidal-Henriquez, Light-matter interaction induces a single positive vortex with swirling arms, Phil. Trans. R. Soc. A **372**, 20140019 (2014).
[17] E. Brasselet, Tunable High-Resolution Macroscopic Self-Engineered Geometric Phase Optical Elements, Phys. Rev. Lett. **121**, 033901 (2018).
[18] G. Milione, H. I. Sztul, D. A. Nolan, and R. R. Alfano, Higher-Order Poincaré Sphere, Stokes Parameters, and the Angular Momentum of Light, Phys. Rev. Lett. **107**, 053601 (2011).
[19] M. Rafayelyan and E. Brasselet, Spin-to-Orbital Angular Momentum Mapping of Polychromatic Light, Phys. Rev. Lett. **120**, 213903 (2018).
[20] T. Wakayama, K. Komaki, Y. Otani, and T. Yoshizawa, Achromatic axially symmetric wave plate, Opt. Express **20**, 29260 (2012).
[21] Y. Li, J. Kim, and M. J. Escuti, Broadband orbital angular momentum manipulation using liquid crystal thin-films, Proc. SPIE Int. Soc. Opt. Eng. **8274**, 827415 (2012).
[22] T. Wakayama, O. G. Rodríguez-Herrera, J. S. Tyo, Y. Otani, M. Yonemura, and T. Yoshizawa, Generation of achromatic, uniform-phase, radially polarized beams, Opt. Express **22**, 3306 (2014).
[23] F. Bouchard, H. Mand, M. Mirhosseini, E. Karimi, and R. W. Boyd, Achromatic orbital angular momentum generator, New J. Phys. **16**, 123006 (2014).
[24] N. Radwell, R. D. Hawley, J. B. Götte, and S. Franke-Arnold, Achromatic vector vortex beams from a glass cone, Nat. Commun. **7**, 10564 (2016).
[25] J. Kobashi, H. Yoshida, and M. Ozaki, Polychromatic Optical Vortex Generation from Patterned Cholesteric Liquid Crystals, Phys. Rev. Lett. **116**, 253903 (2016).
[26] M. Rafayelyan and E. Brasselet, Bragg-berry mirrors: Reflective broadband q-plates, Opt. Lett. **41**, 3972 (2016).
[27] M. Rafayelyan, G. Agez, and E. Brasselet, Ultrabroadband gradient-pitch Bragg-Berry mirrors, Phys. Rev. A **96**, 043862 (2017).
[28] M. Gecevicius, M. Ivanov, M. Beresna, A. Matijosius, V. Tamuliene, T. Gertus, A. Cerkauskaite, K. Redeckas, M. Vengris, V. Smilgevicius, and P. Kazansky, Toward the generation of broadband optical vortices: Extending the spectral range of a q-plate by polarization-selective filtering, J. Opt. Soc. Am. B **35**, 190 (2018).
[29] S. W. Hell and J. Wichmann, Breaking the diffraction resolution limit by stimulated emission: Stimulated-emission-depletion fluorescence microscopy, Opt. Lett. **19**, 780 (1994).
[30] J. Fischer and M. Wegener, Three-dimensional direct laser writing inspired by stimulated-emission-depletion microscopy, Opt. Mater. Express **1**, 614 (2011).
[31] A. M. Weiner, Ultrafast optical pulse shaping: A tutorial review, Opt. Commun. **284**, 3669 (2011).
[32] B. Sun, P. S. Salter, C. Roider, A. Jesacher, J. Strauss, J. Heberle, M. Schmidt, and M. J. Booth, Four-dimensional light shaping: Manipulating ultrafast spatiotemporal foci in space and time, Light Sci. Appl. **7**, 17117 (2018).
[33] B. Alonso, J. Pérez-Vizcaíno, G. Mínguez-Vega, and Í. J. Sola, Tailoring the spatio-temporal distribution of diffractive focused ultrashort pulses through pulse shaping, Opt. Express **26**, 10762 (2018).

[34] K. Murate, M. J. Roshtkhari, X. Ropagnol, and F. Blanchard, Adaptive spatiotemporal optical pulse front tilt using a digital micromirror device and its terahertz application, Opt. Lett. **43**, 2090 (2018).

[35] Ó. Martínez-Matos, P. Vaveliuk, J. Izquierdo, and V. Loriot, Femtosecond spatial pulse shaping at the focal plane, Opt. Express **21**, 25010 (2013).

[36] G. Pariente and F. Quéré, Spatio-temporal light springs: Extended encoding of orbital angular momentum in ultrashort pulses, Opt. Lett. **40**, 2037 (2015).

[37] C. Hernández-García, J. San Román, L. Plaja, and A. Picón, Quantum-path signatures in attosecond helical beams driven by optical vortices, New J. Phys. **17**, 093029 (2015).

[38] J. Arlt and M. J. Padgett, Generation of a beam with a dark focus surrounded by regions of higher intensity: The optical bottle beam, Opt. Lett. **25**, 191 (2000).

[39] E. Brasselet, Babinet-bilayered geometric phase optical elements, Opt. Lett. **43**, 2623 (2018).